

Scrambling and thermalization in a diffusive quantum many-body system

A. Bohrdt,^{1,2} C. B. Mendl,³ M. Endres,⁴ and M. Knap¹

¹*Department of Physics, Walter Schottky Institute, and Institute for Advanced Study, Technical University of Munich, 85748 Garching, Germany*

²*Department of Physics, Harvard University, Cambridge, MA 02138, USA*

³*Stanford Institute for Materials and Energy Sciences,*

SLAC National Accelerator Laboratory, and Stanford University, CA 94025, USA

⁴*Division of Physics, Mathematics and Astronomy, California Institute of Technology, Pasadena, CA 91125, USA*

(Dated: February 21, 2017)

Out-of-time ordered (OTO) correlation functions describe scrambling of information in correlated quantum matter. They are of particular interest in incoherent quantum systems lacking well defined quasi-particles. Thus far, it is largely elusive how OTO correlators spread in incoherent systems with diffusive transport governed by a few globally conserved quantities. Here, we study the dynamical response of such a system using high-performance matrix-product-operator techniques. Specifically, we consider the non-integrable, one-dimensional Bose-Hubbard model in the incoherent high-temperature regime. Our system exhibits diffusive dynamics in time-ordered correlators of globally conserved quantities, whereas OTO correlators display a ballistic, light-cone spreading of quantum information. The slowest process in the global thermalization of the system is thus diffusive, yet information spreading is not inhibited by such slow dynamics. We furthermore develop an experimentally feasible protocol to overcome some challenges faced by existing proposals and to probe time-ordered and OTO correlation functions. Our study opens new avenues for both the theoretical and experimental exploration of thermalization and information scrambling dynamics.

Dynamical correlations of many-body quantum systems provide direct information about many-body excitations [1], describe quantum phases and transitions [2], and characterize certain topological aspects [3, 4]. The dynamical response of a many-body system to a local perturbation is obtained from a time ordered correlation function, $\langle \hat{W}(t)\hat{V}(0) \rangle$, which describes the *relaxation* of the many-body system following the initial excitation by the operator \hat{V} that is then probed at later times by \hat{W} . However, in general such time-ordered correlation functions cannot capture the spread of information across a quantum system, especially in a regime where quasiparticles are not well-defined.

Recently, it has been proposed that spreading or “*scrambling*” of quantum information across all the system’s degrees of freedom can be characterized by out-of-time ordered (OTO) correlation functions: $\langle \hat{W}^\dagger(t)\hat{V}^\dagger(0)\hat{W}(t)\hat{V}(0) \rangle$ [5–10]. These correlation functions appear as the out-of-time ordered part of $\langle |[\hat{W}(t), \hat{V}(0)]|^2 \rangle$ and hence predict the growth of the squared commutator between $\hat{W}(t)$ and $\hat{V}(0)$. OTO correlators are thus capable of describing a quantum analogue of the butterfly effect in classical chaotic systems, which characterizes the spread of local excitations over the whole system. At short times, OTO correlators are expected to grow exponentially with a rate characterized by the Lyapunov exponent λ_L . The Lyapunov exponent has been conjectured to be bounded by $0 \leq \lambda_L \leq 2\pi T$ [9]. This bound is saturated in strongly coupled field theories with a gravity dual [6] and in disordered models describing a strange metal [7, 11, 12]. By contrast, λ_L does not fully saturate the bound for a critical Fermi surface [13] and is parametrically smaller in Fermi liquids or other weakly coupled states [12, 14, 15].

Here, we study both time-ordered and OTO correlators in a diffusive many-body system by considering the concrete example of the non-integrable, one-dimensional Bose-Hubbard model. Thus far, it is a largely open question, how OTO cor-

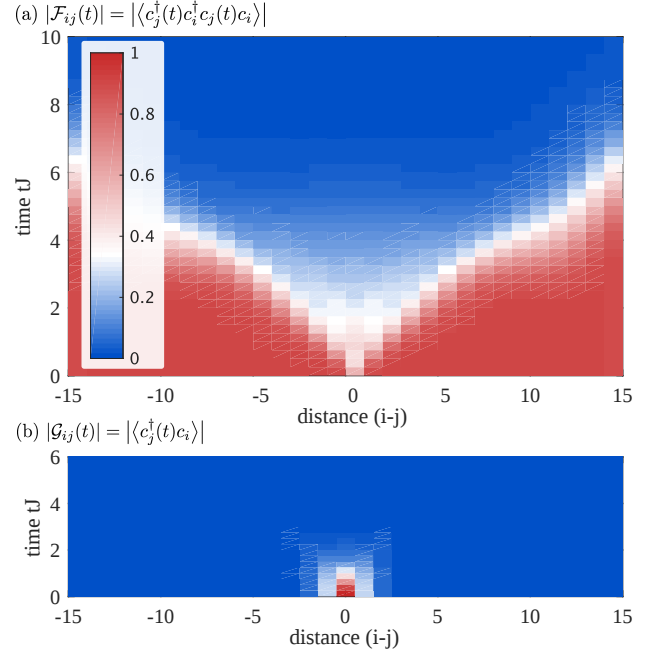


FIG. 1. Dynamical correlation functions in the incoherent transport regime. (a) Out-of-time ordered (OTO) correlators measure the scrambling of information across a quantum state. We compute OTO correlators $\mathcal{F}_{ij}(t) = \langle c_j^\dagger(t)c_i^\dagger c_j(t)c_i \rangle$ in the 1D Bose-Hubbard model at high temperature $T = 4J$ for interactions $U = J$, chemical potential $\mu = 0$, and system size $L = 30$. In the high temperature regime, well-defined quasiparticles cease to exist. However, the OTO correlator \mathcal{F}_{ij} exhibits a light-cone spreading of information. (b) The breakdown of well-defined quasiparticles is demonstrated by the one-particle Green’s function $\mathcal{G}_{ij}(t) = \langle c_j^\dagger(t)c_i \rangle$, which quickly decays to zero within $\tau J \sim 0.6$. The lifetime is thus shorter than the hopping rate, indicating a regime of incoherent transport.

relators spread in diffusive systems with a few globally conserved quantities [10, 13, 15, 16]. In our work, we study this question by performing matrix-product operator (MPO) based simulations of the Bose-Hubbard model at high temperatures, at which well defined quasi-particles cease to exist. We demonstrate that in this regime the time-ordered one-particle correlation functions are strongly incoherent and feature rapidly decaying excitations, whereas the OTO correlators indeed describe the *ballistic* spreading of information across the quantum system (see Fig. 1). In contrast to the linear light-cone spreading of quantum information, the eventual *global* thermalization of the closed system takes parametrically longer, due to hydrodynamic power-laws resulting from globally conserved quantities. For example, we show that the local density correlation function decays as $\sim 1/\sqrt{Dt}$, describing diffusion in one dimension with the corresponding diffusion constant D . Thus, the time scales associated with the spread of information and with global thermalization are different.

Despite their usefulness to characterize interacting many-body systems theoretically, it remains a challenge to experimentally measure such dynamical correlation functions in *real* space and time [17, 18], as required to observe information spreading. Here, we propose generic experimental protocols to characterize both time-ordered and OTO correlators via *local* many-body interferometry. Our proposal to measure OTO correlators is unique because it overcomes some of the challenges that recently proposed protocols exhibit at finite temperatures and because it eliminates the scaling problems associated with *global* many-body interferometry [19, 20]. Furthermore, our protocol does not require an ancillary atom to switch between different system Hamiltonians [21–23] and directly works with massive bosonic and fermionic particles (see also [24–28]). We show that our protocol not only enables the measurement of dynamical correlation functions but also rather generic static correlation functions (including off-diagonal ones), thus opening the way for a full state-tomography of many-body quantum states.

I. RESULTS

We study dynamical correlation functions of the one-dimensional Bose-Hubbard model focusing mainly on the incoherent intermediate to high temperature regime. The Hamiltonian of the system is given by

$$\hat{H} = -J \sum_i (c_i^\dagger c_{i+1} + \text{h.c.}) + \frac{U}{2} \sum_i \hat{n}_i (\hat{n}_i - 1) - \mu \sum_i \hat{n}_i, \quad (1)$$

where J is the tunneling matrix element, U the interaction strength, and μ the chemical potential. The bosonic creation (annihilation) operator on site i is denoted as c_i^\dagger (c_i) and the local particle number operator is $\hat{n}_i = c_i^\dagger c_i$.

At zero temperature and commensurate filling, the Bose-Hubbard model exhibits a quantum phase transition from a gapped Mott insulating phase with short range correlations at strong interactions to a compressible superfluid phase

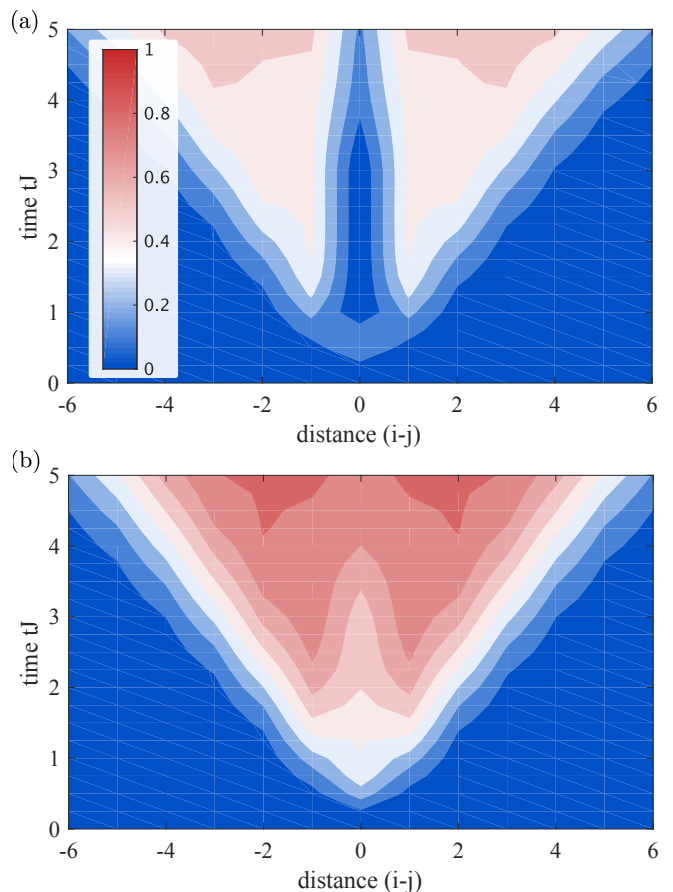


FIG. 2. **Light-cone spreading of quantum information.** Contour plots of the reduced OTO correlator $\mathcal{F}_{ij}^r(t) \sim |\mathcal{F}_{ij}(t) - \langle \hat{n}_i \hat{n}_j \rangle| / \langle \hat{n}_i \hat{n}_j \rangle$ as a function of time and distance for interaction strength $U = J$, chemical potential $\mu = 0$, and temperature (a) $T = 2J$ and (b) $T = 16J$, respectively. The spreading of quantum information forms a light-cone pattern. The contour lines indicate changes of $\mathcal{F}_{ij}^r(t)$ by 0.1.

with power-law correlations at weak interactions [29]. At finite temperatures the system is a correlated, normal fluid. We compute the dynamical correlation functions at finite-temperature for systems up to $L = 50$ sites using MPO techniques. The presented results are evaluated for virtual bond dimension 200 to 400 and the local bosonic Hilbert space is truncated to three states, which is sufficient to render the system nonintegrable. The presented results are checked for convergence with respect to the MPO bond dimension and system size; see Methods III A for details on the numerical simulations.

A. Spread of Quantum Information

Recently, OTO correlation functions have been proposed as a useful diagnostic tool to quantify the dynamical spreading of quantum entanglement and quantum chaos in many-body systems. OTO correlators describe the growth of the commutator

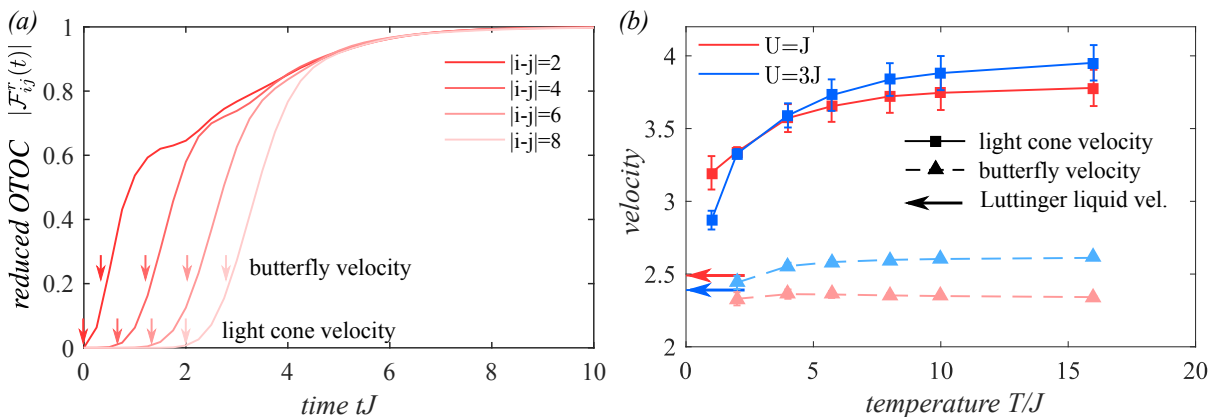


FIG. 3. **Characterizing the speed of information propagation.** (a) Reduced OTO correlators $\mathcal{F}_{ij}^r(t)$ are shown as a function of time for different distances $|i-j|$, interaction strength $U = J$, and temperature $T = 4J$. We introduce the light-cone velocity v_{lc} by the space-time region, where \mathcal{F}^r surpasses a small threshold and the butterfly velocity v_b where it attains a large fraction of order one. (b) The light-cone velocity v_{lc} grows with temperature and is bounded from below by the zero temperature Luttinger liquid velocity (colored arrows). By contrast, the butterfly velocity v_b is systematically smaller than v_{lc} and approximately independent of temperature T . The data is shown for two values of the interaction strength $U = J$ and $U = 3J$.

between two local operators \hat{W} and \hat{V} in time

$$C(t) = -\langle [|\hat{W}(t), \hat{V}(0)|]^2 \rangle. \quad (2)$$

In a semiclassical picture, the commutator in Eq. (2) can be replaced by Poisson brackets. Then, for the choice of $\hat{W} = p_j$ and $\hat{V} = p_i$, this quantity reduces to $C(t) \sim \langle (\partial p_j(t)/\partial q_i(0))^2 \rangle$. Therefore, the correlation function $C(t)$ describes the sensitivity of the time evolution and is expected to grow exponentially at short times $\sim \exp[\lambda_L t]$, with a rate λ_L that resembles the Lyapunov exponent in classical chaotic dynamics. Rewriting these momenta and coordinates as combinations of creation and annihilation operators, Eq. (2) generically consists of OTO correlators of the form

$$\mathcal{F}_{ij}(t) = \langle c_j^\dagger(t) c_i^\dagger c_j(t) c_i \rangle. \quad (3)$$

Below we mainly consider the quantum statistical average $\langle \dots \rangle = \text{tr}[\hat{\rho} \dots]$ over an initial thermal state with weights distributed according to the Gibbs ensemble $\hat{\rho} = e^{-\hat{H}/T}/Z$ where Z is the partition function and we set the Boltzmann constant k_B to one. Alternatively, the average can also be performed with respect to an arbitrary initial state, for example a pure state $\hat{\rho} = |\psi_0\rangle \langle \psi_0|$. For thermalizing systems, it is then expected that an effective temperature is approached at late times which depends on the energy density imprinted on the system by the initial state [30–32].

OTO correlators \mathcal{F}_{ij} evaluated at comparatively high temperatures $T = 4J$, interactions $U = J$, and chemical potential $\mu = 0$ are shown in Fig. 1 (a) as a function of time t and distance $(i-j)$. Despite the high temperature, the OTO correlator \mathcal{F}_{ij} unveils a pronounced light-cone spreading of the information across the quantum state for $|i-j| \lesssim 7$. For larger distances the light cone seems to grow super-ballistically, which we, however, attribute to the finite MPO bond dimension considered in the numerical simulations; see Methods III A. OTO correlators are in that respect challenging to simulate with

MPO techniques, because they directly reflect the fast spreading of entanglement.

The OTO correlator $\mathcal{F}_{ij}(t)$ should be contrasted to the time-ordered single-particle Green's function

$$\mathcal{G}_{ij}(t) = \langle c_j^\dagger(t) c_i \rangle, \quad (4)$$

which is shown in Fig. 1 (b). In the incoherent transport regime, where well-defined quasiparticles do not exist, the Green's function $\mathcal{G}_{ij}(t)$ rapidly decays in time. Therefore, it is not capable of characterizing the spread of quantum information or entanglement across the state which is generically not linked to the transport of quasi-particles [33]. For the chosen parameters ($U = J$, $\mu = 0$, $T = 4J$), we find that the quasi-particle lifetime is approximately $\tau J \sim 0.6$ and hence shorter than the microscopic hopping rate, which indicates incoherent transport. By contrast, the out-of-time ordered structure of $\mathcal{F}_{ij}(t)$ reveals a well defined linear spread of quantum information despite the high temperature.

We now characterize the OTO correlators $\mathcal{F}_{ij}(t)$ in detail. To this end, we subtract $\langle \hat{n}_i \hat{n}_j \rangle$ from the $\mathcal{F}_{ij}(t)$ and consider its relative change: $\mathcal{F}_{ij}^r(t) = |\mathcal{F}_{ij}(t) - \langle \hat{n}_i \hat{n}_j \rangle| / \langle \hat{n}_i \hat{n}_j \rangle$. Examples for the reduced OTO correlator $\mathcal{F}_{ij}^r(t)$ are shown in Fig. 2 for interaction $U = J$ and different temperatures T . The reduced OTO correlator $\mathcal{F}_{ij}^r(t)$ starts off at zero, forms the light-cone plateau, and approaches the steady-state value as an exponential.

From the light-cone spread of the OTO correlator, we extract two velocities [Fig. 3 (a)]: (1) The light-cone velocity v_{lc} , which we define by the space-time region where the reduced OTO correlators $\mathcal{F}_{ij}^r(t)$ surpasses a small threshold of 0.05% of its final value. (2) The butterfly velocity v_b , which we define by the space-time region where the OTO correlator attains a large fraction (20%) of its final value. We find that v_b does not significantly depend on this cutoff, as long as it is chosen to a sizeable fraction; see Methods Fig. 7. The light cone velocity v_{lc} increases with temperature T and is bounded

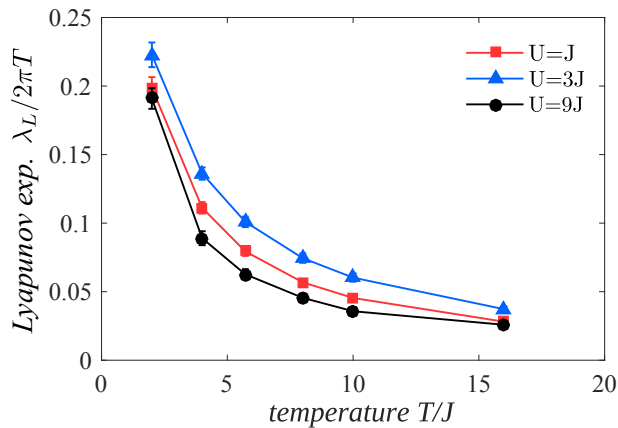


FIG. 4. **Lyapunov exponent.** The reduced OTO correlator $\mathcal{F}_{ij}^r(t)$ is expected to grow exponentially on a timescale set by the butterfly velocity v_b with a rate that defines the Lyapunov exponent λ_L . In our system, the regime of exponential growth is restricted to a rather small time range, see also Fig. 8. Our data suggests that the Lyapunov exponent λ_L is parametrically smaller than the conjectured upper bound $2\pi T$ and increases slowly as the temperature T is lowered. The data is shown for interaction strength $U = \{1, 3, 9\}J$.

from below by the zero temperature Luttinger liquid velocity; see Fig. 3 (b). The butterfly velocity v_b is systematically lower than v_{lc} and is almost independent of temperature. The butterfly velocity determines the time scale t_{scr} for scrambling information across the many-body quantum state which is linear in system size $t_{scr} \sim L/v_b$. Based on results from holography, it has been argued in Ref. [16] that the light-cone and the butterfly velocity should be quite generally the same. This should be contrasted to our results for the Bose-Hubbard model and to a study of non-relativistic non-Fermi liquids [13]. In both cases the butterfly velocity has been found to be smaller than the light-cone velocity. For details on the analysis of the OTO correlators; see Methods III B.

We characterize the initial dynamics of the OTO correlator by its growth rate λ_L around the space-time cone set by the butterfly velocity: $\mathcal{F}_x^r(t) \sim \exp[\lambda_L(t - x/v_b)]$ and refer to this rate as Lyapunov exponent. However, we note that in contrast with predictions from strongly coupled field theories [9] or disordered SYK models [7], there appears to be no parametrically large regime of exponential growth in our model, see Fig. 8, which hints at more complex initial dynamics. Finding the analytic form for the initial growth over an extended space-time region remains an outstanding challenge. Alternatively, one can extract the growth rate Λ_{lc} of the reduced OTO correlator around a space-time region set by the light-cone velocity v_{lc} which we find to be larger than λ_L ; see Methods III B. We show the Lyapunov exponent λ_L as a function of temperature for different values of the interaction strength U and chemical potential $\mu = 0$ in Fig. 4. It has been conjectured that the Lyapunov exponent is bounded by $2\pi T$, which is the value it assumes in a strongly coupled field theory with a gravity dual [9]. In our system, λ_L is parametrically lower than this bound and increases slowly when lowering the temperature. Moreover, we find that the depen-

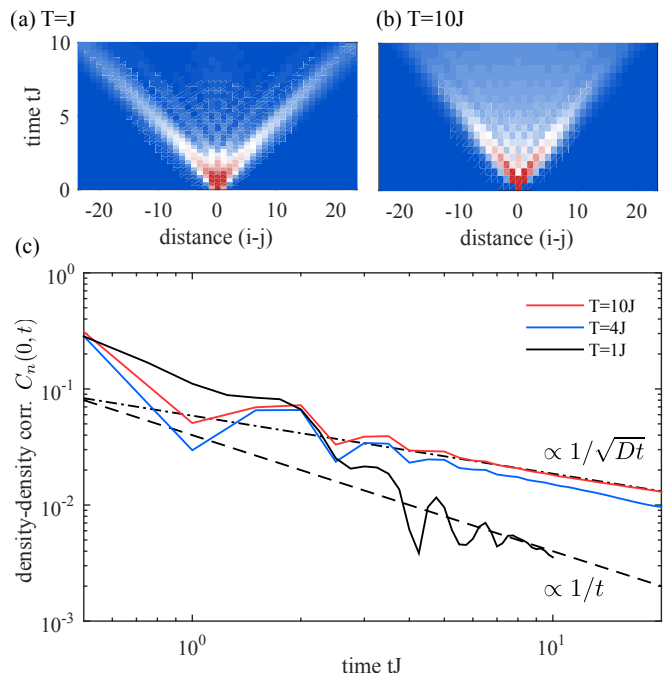


FIG. 5. **Thermalization in closed quantum systems.** Conserved quantities restrict the approach of a closed quantum system to global equilibrium, thus, rendering global thermalization a slow process. In the Bose-Hubbard model the total particle number is conserved leading to diffusive power-law tails in the connected density correlator $C_n(x, t) = \text{Re}[\langle \hat{n}_x(t)\hat{n}_0 \rangle - \langle \hat{n}_x \rangle \langle \hat{n}_0 \rangle]$. (a) At low temperatures ($T = J$), where quasiparticles are reasonably well defined, the density correlator does not reach the diffusive regime within the accessible simulation time but is dominated by ballistic sound peaks. (b) By contrast, for high temperatures ($T = 10J$) the crossover to diffusion becomes apparent. (c) For temperatures $T \gtrsim 4J$ the local density correlator $C_n(0, t) \sim 1/\sqrt{Dt}$, where D is the diffusion constant. By contrast, at low temperature $T = J$ the diffusive regime has not yet been reached within the numerically accessible times and the correlations rather decay ballistically $C_n(0, t) \sim 1/t$. The slow relaxation of the hydrodynamic modes leads to the global thermalization time scale $t_{th} \sim L^2/D$ that is parametrically larger than the scrambling time scale $t_{scr} \sim L/v_b$ of quantum information.

dence of the Lyapunov exponent on the interaction strength U is small with slightly larger values of λ_L for intermediate interaction strength, $U = 3J$, which is in the vicinity of the quantum critical point.

B. Thermalization

Closed quantum systems approach their global equilibrium only very slowly, due to the slow evolution of observables that overlap with conserved quantities. In the Bose-Hubbard model (1), energy, lattice momentum, and total particle number are conserved. From hydrodynamics we infer that, for example, the conserved particle number leads to a diffusion equation of the density [34, 35]

$$\partial_t n - D\nabla^2 n = 0, \quad (5)$$

T/J	$D/(a^2J)$	$D\lambda_L/v_b^2$
4	14.29(27)	7.2(6)
6	11.69(10)	6.0(4)
8	10.42(04)	5.4(3)
10	9.79(01)	5.1(3)

TABLE I. Diffusion constant D and the ratio $D\lambda_L/v_b^2$ for different temperatures T . The errors as indicated in the parentheses are errors from the fits.

where D is the diffusion constant. The connected density correlation function $C_n(x - x', t - t') = \text{Re}[\langle n(x, t)n(x', t') \rangle - \langle n(x) \rangle \langle n(x') \rangle]$ relates the density at space-time (x, t) to the density at (x', t') via $n(x, t) \sim \int dt' dx' C_n(x - x', t - t')n(x', t')$ and in a hydrodynamic regime is expected to be of the form

$$C_n(x, t) \cong \frac{\tilde{C}}{\sqrt{4\pi D|t|}} e^{-\frac{x^2}{4D|t|}}, \quad (6)$$

with $\tilde{C} = \int dx C_n(x, 0)$. Whereas local equilibrium is approached after a few scattering events, attaining global equilibrium is restricted due to the relaxation of such conserved quantities, which have to be transported over long distances. At comparatively low temperatures ($T = J$), Fig. 5 (a), the ballistic spread of sound modes dominates the dynamics of the connected density correlator in the numerically accessible time regime. However, at high temperatures ($T = 10J$), (b), the density correlator approaches diffusive transport after a few hopping scales and attains a finite value in the region between the sound modes. To be more quantitative, we study the local ($x - x' = 0$) density correlation function. At high temperatures $T \gtrsim 4J$ the local correlator exhibits a diffusive power-law decay $C_n(x = 0, t) \sim 1/\sqrt{Dt}$, (c). For this parameter set we extract the diffusion constant $D = 9.79(1)a^2J$ for $T = 10J$ and $D = 14.29(27)a^2J$ for $T = 4J$, where a is the lattice spacing; see Tab. I. The decrease of the diffusion constant with increasing temperature is somewhat counterintuitive. We attribute this behavior to the fact that the calculations are performed in the grand-canonical ensemble. Hence the particle density depends on the temperature and, in particular, increases with temperature in the chosen parameter regime. We note that the connected density correlator does not exhibit pronounced hydrodynamic long time tails, which could result from higher order gradient corrections to the diffusion equation and mask the $1/\sqrt{Dt}$ decay. This seems to be a particular property of the density correlator, as we find at high-temperatures pronounced $t^{-3/4}$ corrections in the energy-density correlation function (not shown), in agreement with Ref. [35].

It has been proposed that the diffusion constant is related to the butterfly velocity v_b and the Lyapunov exponent λ_L via $D \sim v_b^2/\lambda_L$ [36–39], where $1/\lambda_L$ is a bound for the local thermalization time in which the system is able to attain local equilibrium characterized by a local temperature and local chemical potential that varies between different regions in

space. From our simulations, we obtain coefficients of the order $D\lambda_L/v_b^2 \sim 5.5$ for temperatures $T \gtrsim 6J$; see Tab. I, which seems to suggest a connection between the spread of information and local thermalization, as suggested by calculations for holographic matter. However, clearly global thermalization is a parametrically slower process than information scrambling and takes for systems of size L times of the order $t_{\text{th}} \sim L^2/D$. Experimentally measuring OTO correlators (Sec. IC) and density correlators (App. A3) will make it possible to further check these holographic predictions.

C. Measuring Dynamical Time-Ordered and Out-of-Time Ordered Correlators

We develop two generic interferometric protocols that measure time-ordered as well as OTO correlation functions for systems of bosons or fermions in an optical lattice. The first is based on globally interfering two many-body states and the second on local interference. The quantum interference of two copies of the many-body state is realized by local beam splitter operations. Variants of this approach have been proposed to study Rényi entropies [40–42] and have been demonstrated experimentally using a quantum gas microscope [19, 20]. Both protocols that we propose consist only of elements which have already been used in experiments. The two protocols are complementary and each of them has its own advantages.

Global interferometry precisely yields the square modulus of the single-particle Green's functions $\mathcal{G}_{ij}^{\text{gl}}(t) = |\mathcal{G}_{ij}(t)|^2$ and the OTO correlators $\mathcal{F}_{ij}^{\text{gl}}(t) = |\mathcal{F}_{ij}(t)|^2$ for pure initial states (see Supplemental Information Sec. A1). In a thermalizing system, effective finite temperatures can be obtained with the help of quenches from pure initial states. However, generic high temperature initial states are not accessible with this protocol. The measurement schemes proposed e.g. in Ref. [23] face similar challenges. The global interferometry protocol is furthermore limited to rather small system sizes, since the many-body wave function overlap has to be measured, which requires an extensive number of beam splitter operations.

These limitations are overcome by the second proposed protocol which uses local interferometry (see Supplemental Information Sec. A2 for details on the implementation). In this protocol, only two local beam-splitter operations are required irrespective of the system size, and only local density differences between the two copies have to be measured. Furthermore, initial thermal density matrices can be studied as well. This local approach yields a slightly amended two-point correlation function $\mathcal{G}_{ij}^{\text{loc}}(t) \sim \text{Im}[\langle a_j^\dagger(t)a_i \rangle \langle a_j(t)a_i^\dagger \rangle]$ and OTO correlator $\mathcal{F}_{ij}^{\text{loc}}(t) \sim \text{Im}[\langle a_j^\dagger(t)a_i^\dagger a_j(t)a_i \rangle \langle a_j^\dagger(t)a_i a_j(t)a_i^\dagger \rangle]$. However, we demonstrate in the Supplemental Material that these correlators carry much of the same information as the ones we discussed previously. Static correlation functions are accessible with the same techniques and an extension to higher order correlators is straight forward.

II. DISCUSSION

We studied time-ordered as well as out-of-time ordered correlation functions in the one-dimensional Bose-Hubbard model and suggest different protocols to experimentally access them. At high temperatures, well-defined quasi-particles cease to exist and the time-ordered Green's function decays within short times. However, the spread of information is not necessarily linked to the transport of quasi-particles. Our numerical results for the out-of-time ordered correlators clearly indicate the ballistic spread of information even at high temperatures where transport is incoherent. In our one-dimensional system, this linear spread sets the timescale for scrambling information across the quantum state to be proportional to the system size. Moreover, the existence of conserved quantities in the Bose-Hubbard model leads to diffusive behavior of the corresponding time-ordered correlation functions. Global thermalization therefore scales with the square of the system size and takes parametrically longer than scrambling quantum information.

For future work, it would be on the one hand interesting to develop analytical predictions for the growth of OTO correlators, which in our numerics deviates significantly from the simple exponential growth obtained in strongly coupled field theories, or for the bounds that characterize the information propagation and Lyapunov exponents. On the other hand, the numerical study of out-of-time ordered correlators in other interacting many-body systems, including Fermi-Hubbard models, spin models, or continuum Lieb-Liniger models, could be beneficial. Taking such routes could help to advance our fundamental understanding of information scrambling, transport, and thermalization.

Experimental measurements of both time-ordered and out-of-time ordered correlators will be eminent for the investigation of the dynamical properties of many-body systems. We proposed two different protocols to measure correlation functions, which can be either static, time ordered, or out-of-time ordered. The schemes are respectively based on the global and local interference of two copies of the many-body state of interest. The required techniques have already been demonstrated in experiments with synthetic quantum matter. An extension of the described experimental schemes to two-dimensional systems is conceivable as well and could provide a valuable perspective on the dynamics of many-body quantum systems.

III. METHODS

In this section, we discuss the numerical method with which the calculations have been performed as well as the procedure to obtain the velocities v_{lc} , v_b and the Lyapunov exponent λ_L .

A. Numerical Simulations

Our numerical simulations are based on finite-temperature, time-dependent matrix product operators (MPO) [43–48].

For the density correlations, we evaluate [47]

$$\begin{aligned} \langle \hat{n}_\ell(t) \hat{n}_j(0) \rangle_\beta &\stackrel{\text{def}}{=} \frac{1}{Z} \text{tr} \left[e^{-\beta \hat{H}} (e^{it\hat{H}} \hat{n}_\ell e^{-it\hat{H}}) \hat{n}_j \right] \\ &= \frac{1}{Z} \text{tr} \left[(e^{i\frac{t}{2}\hat{H}} e^{-\beta\hat{H}/2} \hat{n}_\ell e^{-i\frac{t}{2}\hat{H}}) (e^{-i\frac{t}{2}\hat{H}} \hat{n}_j e^{-\beta\hat{H}/2} e^{i\frac{t}{2}\hat{H}}) \right], \end{aligned} \quad (7)$$

where β is the inverse temperature and Z the partition function. We construct the MPO approximation of the two terms in the parentheses by first computing $e^{-\beta\hat{H}/2} \hat{n}_\ell$ and $\hat{n}_j e^{-\beta\hat{H}/2}$, respectively, and then performing a real-time evolution up to $\frac{t}{2}$ and $-\frac{t}{2}$. By exploiting the time translation invariance, $\langle \hat{n}_\ell(t) \hat{n}_j(0) \rangle_\beta = \langle \hat{n}_\ell(t/2) \hat{n}_j(-t/2) \rangle_\beta$, the maximum simulated time has effectively been reduced by a factor two, which in turn reduces the required virtual bond dimension of the MPO.

To evaluate $e^{-\beta\hat{H}/2}$, we employ a second-order Suzuki-Trotter decomposition with imaginary time step $\Delta\tau$ (typically $\Delta\tau J = 0.025$) after splitting the Hamiltonian into even and odd bonds, as described in Ref. 43. The real-time evolution proceeds by Liouville steps $\hat{A}(t + \Delta t) = e^{i\Delta t \hat{H}} \hat{A}(t) e^{-i\Delta t \hat{H}}$. For each of the steps we combine a fourth-order partitioned Runge-Kutta method [49] with even-odd bond splitting of the Hamiltonian. As noted in Ref. 47, the Liouville time evolution has the advantage that the virtual bond dimension does not increase outside the space-time cone set by Lieb-Robinson-type bounds. The high order decomposition also allows for relatively large time steps (in our case $\Delta t J = 0.125$ or 0.25).

For the OTO correlators $\langle c_j^\dagger(t) c_\ell^\dagger c_j(t) c_\ell \rangle_\beta$, a regrouping analogous to Eq. (7) would lead to four terms inside the trace, such that a straightforward contraction to evaluate the trace becomes computationally very expensive. Instead, we evaluate

$$\begin{aligned} \langle c_j^\dagger(t) c_\ell^\dagger c_j(t) c_\ell \rangle_\beta \\ = \frac{1}{Z} \text{tr} \left[(e^{it\hat{H}} e^{-\beta\hat{H}} c_j^\dagger e^{-it\hat{H}} c_\ell^\dagger) (e^{it\hat{H}} c_j e^{-it\hat{H}} c_\ell) \right] \end{aligned} \quad (8)$$

and time-evolve both $e^{-\beta\hat{H}} c_j^\dagger$ and c_j up to time t . Subsequent application of the site-local operators c_ℓ^\dagger and c_ℓ does not affect the virtual bond dimension in the MPO representation.

In our simulations, we restrict the local Hilbert space to three states due to computational limitations. Since the average particle number per site is approximately one, this restriction should not qualitatively affect the simulation results. Moreover, truncating the local Hilbert space to three states is sufficient to render the system non-integrable, which is crucial to observe the thermalization behavior studied in this work.

Since OTO correlators are closely linked to the spreading of entanglement, it is challenging to simulate them using MPO techniques. In Fig. 6 we compare the data obtained for the same simulation parameters but different maximal bond dimensions. The MPO bond dimension of 20 leads to an apparently super-ballistic growth of the light-cone around $|i - j| \approx 5$, see Fig. 6(a). Increasing the bond dimension shifts this numerical artifact to larger distances. It is however exponentially costly to reach full convergence of the OTO correlator. In the analysis of the numerical data we therefore only

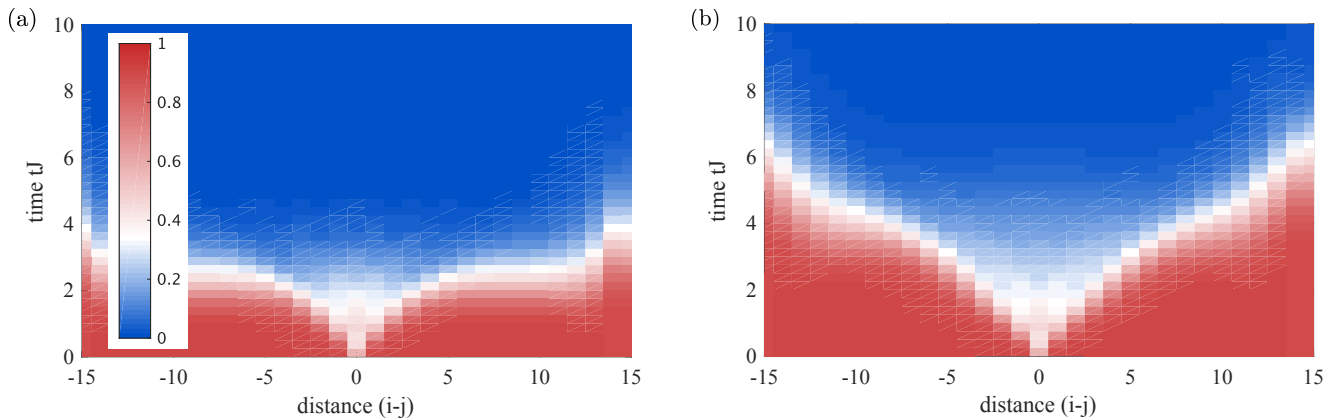


FIG. 6. **Comparison of numerical data for different bond dimensions.** OTO correlators $\mathcal{F}_{ij}^r(t)$ are shown for $T = 4J$ and $U = J$, and bond dimension (a) 20 and (b) 400. The plateau emerging around $|i - j| \approx 5$ in (a) diminishes and appears only at larger distances for the higher bond dimension shown in (b). However, despite the large difference in the bond dimension, deviations from the linear light cone are still apparent.

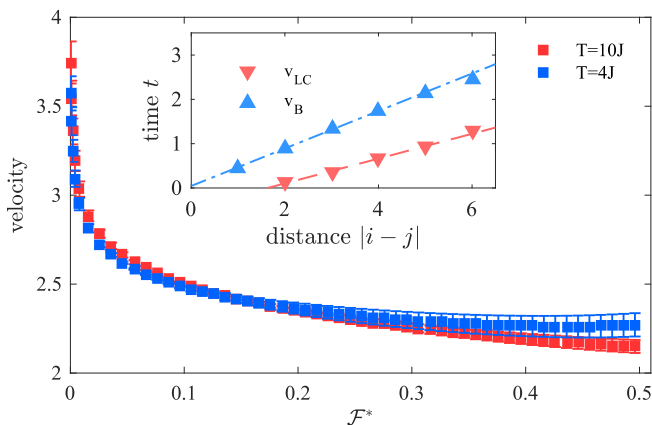


FIG. 7. **Determining the light-cone v_{lc} and butterfly velocity v_b .** The velocities resulting from a linear fit to the times at which $\mathcal{F}_{ij}^r(t)$ reaches the value \mathcal{F}^* are shown for $U = J$ and $T = \{4, 10\}J$. The errorbars are the fitting errors. Inset: The inverse slope of the linear fit to the times as a function of distance $|i - j|$ determines the different velocities (shown for $U = J$ and $T = 4J$).

considered small distances, where we checked that increasing the bond dimension does not alter the correlators.

B. Data Analysis

We describe in detail, how we determine the light-cone velocity v_{lc} , the butterfly velocity v_b , and the Lyapunov exponent λ_L . The light-cone velocity is defined as the ratio of the distance $|i - j|$ and the time at which the reduced OTO correlator $\mathcal{F}_{ij}^r(t)$ reaches a small threshold. The butterfly velocity, however, sets a scale for the time it takes to scramble information over the system and is therefore defined via the time at which $\mathcal{F}_{ij}^r(t)$ attains a large value of order one. The specific threshold one chooses to determine the butterfly velocity is thus somewhat arbitrary. We illustrate the dependence of

the velocity v on the chosen threshold \mathcal{F}^* of the reduced OTO correlator $\mathcal{F}_{ij}^r(t)$ in Fig. 7. For large values of \mathcal{F}^* , the velocity converges toward a constant. Hence, the butterfly velocity will be largely insensitive to the precise choice of \mathcal{F}^* as long as it is large enough. For the definition of v_b , we consider the specific value of $\mathcal{F}_b^* = 0.2$.

In the limit $\mathcal{F}^* \rightarrow 0$, there is a strong dependence of v on the choice of the threshold. The light-cone velocity v_{lc} is defined by the fastest spread of information through the system and is determined by the reduced OTO correlator attaining a small value. To fulfill this definition, we fix $\mathcal{F}_{lc}^* = 0.0005$; see inset in Fig. 7.

As described in Sec. IA, the OTO correlator is expected to grow exponentially on a timescale set approximately by the butterfly velocity. We thus fit the exponential function

$$\mathcal{F}_x^r(t) = a \cdot e^{\lambda_L \left(t - \frac{x}{v_b}\right)} \quad (9)$$

to the numerical data simultaneously for distances $1 \leq |i - j| \leq 5$ within the range $-2.5 \leq \log \mathcal{F}_{ij}^r(t) \leq -1$. The butterfly velocity v_b is determined as described above with the threshold $\mathcal{F}^* = 0.2$, which lies well within the interval of the considered data points; see Fig. 8(a) for an exemplary plot.

We note that the exponential growth of the reduced OTO correlator is in our model limited to a rather small dynamical range. Extracting by contrast the growth rate Λ_{lc} of the OTO correlator from the timescale set by the light-cone velocity within the range $-14 \leq \log \mathcal{F}_{ij}^r(t) \leq -4.5$, Fig. 8(b), yields larger rates. In particular, for the parameters shown in Fig. 8, we obtain $\lambda_L = 2.9(1)$ and $\Lambda_{lc} = 10.3(5)$, respectively.

ACKNOWLEDGMENTS

We thank T. Barthel, X. Chen, S. Gopalakrishnan, H.-C. Jiang, A. Kitaev, and S. Sachdev for useful discussions. We acknowledge support from the Technical University of

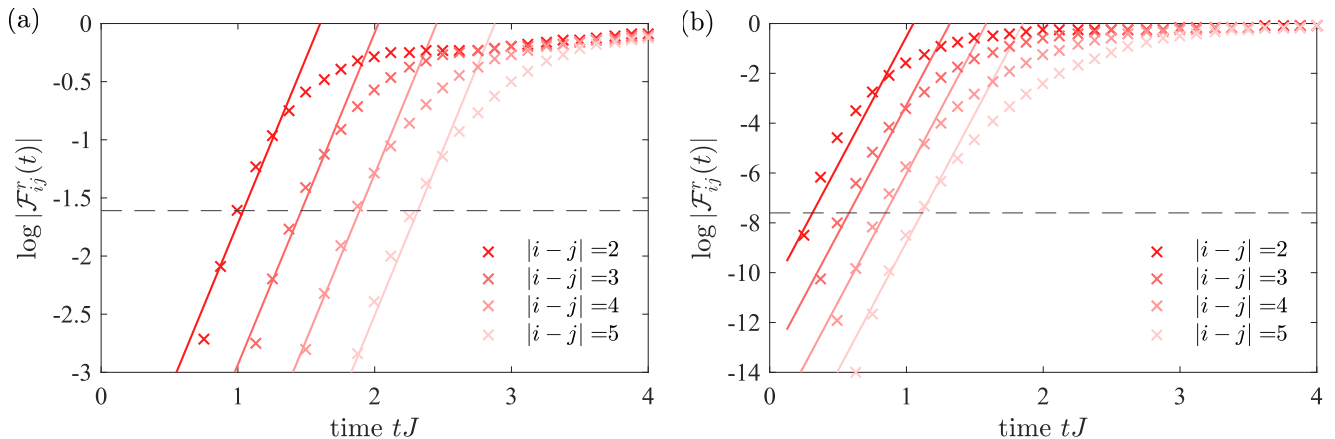


FIG. 8. **Determining the Lyapunov exponent λ_L .** OTO correlators $\mathcal{F}_{ij}^r(t)$ are shown for $T = 10J$ and $U = J$. Solid lines depict the predicted exponential growth from which we determine (a) the Lyapunov exponent $\lambda_L = 2.9(1)$ and (b) the light-cone exponent $\Lambda_{lc} = 10.3(5)$. The dashed gray line denotes the threshold value \mathcal{F}^* used to determine the velocities v_b and v_{lc} , respectively. We obtain the exponents by fitting our data in a restricted regime around the threshold value \mathcal{F}^* to the predicted exponential growth, see text for details. However, we note that in our data the exponential growth is limited to a rather small time range. The errorbars shown in Fig. 4 correspond to errors obtained from such fits.

Munich - Institute for Advanced Study, funded by the German Excellence Initiative and the European Union FP7 under grant agreement 291763 (A.B, M.K), the DFG grant No.

KN 1254/1-1 (A.B, M.K), the Studienstiftung des deutschen Volkes (A.B.), and the Alexander von Humboldt foundation via a Feodor Lynen fellowship (C.M.).

-
- [1] Alexander L. Fetter and John Dirk Walecka, *Quantum Theory of Many-Particle Systems* (McGraw-Hill, New York, 1971).
- [2] Subir Sachdev, *Quantum Phase Transitions*, 2nd ed. (Cambridge University Press, Cambridge, England, 2011).
- [3] Matthias Punk, Debanjan Chowdhury, and Subir Sachdev, “Topological excitations and the dynamic structure factor of spin liquids on the kagome lattice,” *Nat. Phys.* **10**, 289–293 (2014).
- [4] Siddhardh C. Morampudi, Ari M. Turner, Frank Pollmann, and Frank Wilczek, “Statistics of fractionalized excitations through threshold spectroscopy,” [arXiv:1608.05700](https://arxiv.org/abs/1608.05700) (2016).
- [5] Larkin A.I. and Ovchinnikov Yu. N., “Quasiclassical method in the theory of superconductivity,” *JETP Lett.* **28**, 1200 (1969).
- [6] Stephen H. Shenker and Douglas Stanford, “Black holes and the butterfly effect,” *J. High Energy Phys.* **2014**, 67 (2014).
- [7] A. Y. Kitaev, “A simple model of quantum holography,” *KITP Program on Entanglement in Strongly-Correlated Quantum Matter* (2015).
- [8] Daniel A. Roberts, Douglas Stanford, and Leonard Susskind, “Localized shocks,” *J. High Energy Phys.* **2015**, 51 (2015).
- [9] Juan Maldacena, Stephen H. Shenker, and Douglas Stanford, “A bound on chaos,” *J. High Energy Phys.* **2016**, 106 (2016).
- [10] Pavan Hosur, Xiao-Liang Qi, Daniel A. Roberts, and Beni Yoshida, “Chaos in quantum channels,” *J. High Energy Phys.* **2016**, 4 (2016).
- [11] Subir Sachdev and Jinwu Ye, “Gapless spin-fluid ground state in a random quantum Heisenberg magnet,” *Phys. Rev. Lett.* **70**, 3339–3342 (1993).
- [12] Sumilan Banerjee and Ehud Altman, “Solvable model for a dynamical quantum phase transition from fast to slow scrambling,” [arXiv:1610.04619](https://arxiv.org/abs/1610.04619) (2016).
- [13] Aavishkar A. Patel and Subir Sachdev, “Quantum chaos on a critical Fermi surface,” [arXiv:1611.00003](https://arxiv.org/abs/1611.00003) (2016).
- [14] Douglas Stanford, “Many-body chaos at weak coupling,” *J. High Energy Phys.* **2016**, 9 (2016).
- [15] Igor L. Aleiner, Lara Faoro, and Lev B. Ioffe, “Microscopic model of quantum butterfly effect: out-of-time-order correlators and traveling combustion waves,” [arXiv:1609.01251](https://arxiv.org/abs/1609.01251) (2016).
- [16] Márk Mezei and Douglas Stanford, “On entanglement spreading in chaotic systems,” [arXiv:1608.05101](https://arxiv.org/abs/1608.05101) (2016).
- [17] Michael Knap, Adrian Kantian, Thierry Giamarchi, Immanuel Bloch, Mikhail D. Lukin, and Eugene Demler, “Probing real-space and time-resolved correlation functions with many-body Ramsey interferometry,” *Phys. Rev. Lett.* **111**, 147205 (2013).
- [18] M. Serbyn, M. Knap, S. Gopalakrishnan, Z. Papi, N.Y. Yao, C.R. Laumann, D.A. Abanin, M.D. Lukin, and E.A. Demler, “Interferometric probes of many-body localization,” *Phys. Rev. Lett.* **113**, 147204 (2014).
- [19] Rajibul Islam, Ruichao Ma, Philipp M. Preiss, M. Eric Tai, Alexander Lukin, Matthew Rispoli, and Markus Greiner, “Measuring entanglement entropy in a quantum many-body system,” *Nature* **528**, 77–83 (2015).
- [20] Adam M. Kaufman, M. Eric Tai, Alexander Lukin, Matthew Rispoli, Robert Schittko, Philipp M. Preiss, and Markus Greiner, “Quantum thermalization through entanglement in an isolated many-body system,” *Science* **353**, 794–800 (2016).
- [21] Brian Swingle, Gregory Bentsen, Monika Schleier-Smith, and Patrick Hayden, “Measuring the scrambling of quantum information,” *Phys. Rev. A* **94**, 040302 (2016).
- [22] Guanyu Zhu, Mohammad Hafezi, and Tarun Grover, “Measurement of many-body chaos using a quantum clock,” *Phys.*

- Rev. A **94**, 062329 (2016).
- [23] Norman Y. Yao, Fabian Grusdt, Brian Swingle, Mikhail D. Lukin, Dan M. Stamper-Kurn, Joel E. Moore, and Eugene A. Demler, “Interferometric Approach to Probing Fast Scrambling,” [arXiv:1607.01801](#) (2016).
- [24] Huitao Shen, Pengfei Zhang, Ruihua Fan, and Hui Zhai, “Out-of-Time-Order Correlation at a Quantum Phase Transition,” [arXiv:1608.02438](#) (2016).
- [25] Naoto Tsuji, Philipp Werner, and Masahito Ueda, “Exact out-of-time-ordered correlation functions for an interacting lattice fermion model,” *Phys. Rev. A* **95**, 011601 (2017).
- [26] Daniel A. Roberts and Brian Swingle, “Lieb-Robinson Bound and the Butterfly Effect in Quantum Field Theories,” *Phys. Rev. Lett.* **117**, 091602 (2016).
- [27] Nicole Yunger Halpern, “Jarzynski-like equality for the out-of-time-ordered correlator,” [arXiv:1609.00015](#) (2016).
- [28] Michele Campisi and John Goold, “Thermodynamics of quantum information scrambling,” [arXiv:1609.05848](#) (2016).
- [29] Thierry Giamarchi, *Quantum Physics in One Dimension* (Oxford University Press, Oxford, 2004).
- [30] J. M. Deutsch, “Quantum statistical mechanics in a closed system,” *Phys. Rev. A* **43**, 2046–2049 (1991).
- [31] Mark Srednicki, “Chaos and quantum thermalization,” *Phys. Rev. E* **50**, 888–901 (1994).
- [32] Marcos Rigol, Vanja Dunjko, and Maxim Olshanii, “Thermalization and its mechanism for generic isolated quantum systems,” *Nature (London)* **452**, 854–858 (2008).
- [33] Hyungwon Kim and David A. Huse, “Ballistic Spreading of Entanglement in a Diffusive Nonintegrable System,” *Phys. Rev. Lett.* **111**, 127205 (2013).
- [34] P. M. Chaikin and T. C. Lubensky, *Principles of Condensed Matter Physics* (Cambridge University Press, Cambridge; New York, USA, 2000).
- [35] Jonathan Lux, Jan Müller, Aditi Mitra, and Achim Rosch, “Hydrodynamic long-time tails after a quantum quench,” *Phys. Rev. A* **89**, 053608 (2014).
- [36] Mike Blake, “Universal Charge Diffusion and the Butterfly Effect in Holographic Theories,” *Phys. Rev. Lett.* **117**, 091601 (2016).
- [37] Sean A. Hartnoll, “Theory of universal incoherent metallic transport,” *Nat. Phys.* **11**, 54–61 (2015).
- [38] Brian Swingle and Debanjan Chowdhury, “Slow scrambling in disordered quantum systems,” [arXiv:1608.03280](#) (2016).
- [39] Andrew Lucas and Julia Steinberg, “Charge diffusion and the butterfly effect in striped holographic matter,” *J. High Energy Phys.* **2016**, 143 (2016).
- [40] C. Moura Alves and D. Jaksch, “Multipartite Entanglement Detection in Bosons,” *Phys. Rev. Lett.* **93**, 110501 (2004).
- [41] A. J. Daley, H. Pichler, J. Schachenmayer, and P. Zoller, “Measuring Entanglement Growth in Quench Dynamics of Bosons in an Optical Lattice,” *Phys. Rev. Lett.* **109**, 020505 (2012).
- [42] Hannes Pichler, Lars Bonnes, Andrew J. Daley, Andreas M. Läuchli, and Peter Zoller, “Thermal versus entanglement entropy: a measurement protocol for fermionic atoms with a quantum gas microscope,” *New J. Phys.* **15**, 063003 (2013).
- [43] S. R. White and A. E. Feiguin, “Real-time evolution using the density matrix renormalization group,” *Phys. Rev. Lett.* **93**, 076401 (2004).
- [44] F. Verstraete, J. J. García-Ripoll, and J. I. Cirac, “Matrix product density operators: Simulation of finite-temperature and dissipative systems,” *Phys. Rev. Lett.* **93**, 207204 (2004).
- [45] F. Verstraete, V. Murg, and J. I. Cirac, “Matrix product states, projected entangled pair states, and variational renormalization group methods for quantum spin systems,” *Adv. Phys.* **57**, 143–224 (2008).
- [46] U. Schollwöck, “The density-matrix renormalization group in the age of matrix product states,” *Ann. Phys.* **326**, 96–192 (2011).
- [47] T. Barthel, “Precise evaluation of thermal response functions by optimized density matrix renormalization group schemes,” *New J. Phys.* **15**, 073010 (2013).
- [48] C. Karrasch, J. H. Bardarson, and J. E. Moore, “Reducing the numerical effort of finite-temperature density matrix renormalization group transport calculations,” *New J. Phys.* **15**, 083031 (2013).
- [49] S. Blanes and P. C. Moan, “Practical symplectic partitioned Runge-Kutta and Runge-Kutta-Nyström methods,” *J. Comput. Appl. Math.* **142**, 313–330 (2002).
- [50] S. Braun, J. P. Ronzheimer, M. Schreiber, S. S. Hodgman, T. Rom, I. Bloch, and U. Schneider, “Negative Absolute Temperature for Motional Degrees of Freedom,” *Science* **339**, 52–55 (2013).
- [51] H. Lignier, C. Sias, D. Ciampini, Y. Singh, A. Zenesini, O. Morsch, and E. Arimondo, “Dynamical Control of Matter-Wave Tunneling in Periodic Potentials,” *Phys. Rev. Lett.* **99**, 220403 (2007).
- [52] Daniel F. V. James, Paul G. Kwiat, William J. Munro, and Andrew G. White, “Measurement of qubits,” *Phys. Rev. A* **64**, 052312 (2001).
- [53] D. Clément, N. Fabbri, L. Fallani, C. Fort, and M. Inguscio, “Exploring correlated 1D Bose gases from the superfluid to the Mott-insulator state by inelastic light scattering,” *Phys. Rev. Lett.* **102**, 155301 (2009).
- [54] Philipp T. Ernst, Soren Gotze, Jasper S. Krauser, Karsten Pyka, Dirk-Soren Luhmann, Daniela Pfannkuche, and Klaus Sengstock, “Probing superfluids in optical lattices by momentum-resolved Bragg spectroscopy,” *Nat Phys* **6**, 56–61 (2010).

Supplemental Information

Appendix A: Details on the Experimental Protocols

We elaborate on the different protocols outlined in Sec. IC, which can be used to experimentally access the theoretical findings presented in this work.

1. Global Many-Body Interferometry

We consider a system of bosons or fermions in an optical lattice. At this point, we do not make any assumptions about the specific form of the Hamiltonian \hat{H} . We first focus on the real-time and spatially resolved single-particle Green's functions $\mathcal{G}_{ij}^{\text{gl}}(t)$, which can be measured by the following protocol, Fig. 9(a): (1) Initially, prepare two identical copies of a pure state $|\psi\rangle \otimes |\psi\rangle$. Remove a particle on site i in the left system by locally transferring the atom to a hyperfine state that is decoupled from the rest of the system or by transferring it to a higher band of the optical lattice, yielding $c_i |\psi\rangle \otimes |\psi\rangle$. (2) The system evolves in time for a period t , $\exp[-i\hat{H}t]c_i |\psi\rangle \otimes \exp[-i\hat{H}t] |\psi\rangle$. (3) Create a hole on site j of the right system

$$|\psi_l(t)\rangle \otimes |\psi_r(t)\rangle \equiv e^{-i\hat{H}t} c_i |\psi\rangle \otimes c_j e^{-i\hat{H}t} |\psi\rangle. \quad (\text{A1})$$

We abbreviate the sequence of the operations (1–3) as $\hat{O}(i, j)$ and illustrate the corresponding quantum circuit in the bottom of the blue box in Fig. 9(a). (4) Finally, measure the swap operator $\hat{\mathcal{V}}$, which interchanges the particles between the left and the right subsystem

$$\begin{aligned} \langle \hat{\mathcal{V}} \rangle &= \text{tr}[|\psi_r(t)\rangle \langle \psi_l(t)| \otimes |\psi_l(t)\rangle \langle \psi_r(t)|] \\ &= |\langle \psi_r(t) | \psi_l(t) \rangle|^2 = |\langle c_j^\dagger(t) c_i \rangle|^2 = \mathcal{G}_{ij}^{\text{gl}}(t). \end{aligned} \quad (\text{A2})$$

The expectation value of the swap operator is experimentally determined by a global 50%-50% beam splitter operation, which is realized by tunnel-coupling the left and the right system, followed by a measurement of the parity-projected particle number [19, 40, 41].

OTO correlation functions are measured in a similar fashion, Fig. 9b. To begin with, we recycle the first three steps of the Green's function protocol, compiled in $\hat{O}(i, j)$. As a second step, the sign of the Hamiltonian needs to be inverted globally. The sign of the interaction can be flipped by ramping the magnetic field across a Feshbach resonance, as demonstrated experimentally, for instance, in the realization of negative temperature states [50]. Furthermore, by appropriately tuning the drive frequency of a modulated optical lattice, the sign of the hopping matrix element can be flipped [51]. Combining these already established experimental techniques, the global sign of the Hamiltonian is inverted. As a next step, the operations $\hat{O}(j, i)$ are applied again, leading to the time

evolved state

$$|\psi_l(t)\rangle \otimes |\psi_r(t)\rangle \equiv e^{i\hat{H}t} c_j e^{-i\hat{H}t} c_i |\psi\rangle \otimes c_i e^{i\hat{H}t} c_j e^{-i\hat{H}t} |\psi\rangle. \quad (\text{A3})$$

The square modulus of the OTO correlators is then obtained by measuring the wavefunction overlap of the left and the right system using beam splitters as discussed before.

For the measurement of both the Green's function and the OTO correlators, the initial state $|\psi\rangle$ can be an arbitrary pure state, such as the ground state, or a simple product state. An effective finite temperature state can be obtained for quenches from initial pure states to some final Hamiltonian. In a thermalizing system [30–32], the effective temperature is then determined by the energy-density produced by the quantum quench. In the case of a thermal initial state, after the first three steps of our protocol, blue box in Fig. 9, the system is prepared in the state $\rho_l(t) \otimes \rho_r(t)$, where $\rho_\alpha(t)$ is a generic density matrix. The measurement of the swap operator $\hat{\mathcal{V}}$ yields [41]

$$\begin{aligned} \langle \hat{\mathcal{V}} \rangle &= \text{tr} \hat{\mathcal{V}} \rho_l(t) \otimes \rho_r(t) \\ &= \text{tr} \hat{\mathcal{V}} \sum_{\mu\nu} \rho_{l,\mu}(t) \rho_{r,\nu}(t) |\mu\rangle \langle \mu| \otimes |\nu\rangle \langle \nu| \\ &= \text{tr} \sum_{\mu\nu} \rho_{l,\mu}(t) \rho_{r,\nu}(t) |\nu\rangle \langle \mu| \otimes |\mu\rangle \langle \nu| \\ &= \sum_{\mu} \rho_{l,\mu}(t) \rho_{r,\mu}(t) = \text{tr} \rho_l(t) \rho_r(t). \end{aligned} \quad (\text{A4})$$

For pure states, $\rho_{l,r}(t) = |\psi_{l,r}(t)\rangle \langle \psi_{l,r}(t)|$, we directly obtain Eq. (A2). However, at finite temperature, the measurement does not directly yield the square of the correlation function. In particular, we obtain for the Green's function protocol

$$\langle \hat{\mathcal{V}} \rangle = \sum_{\mu\nu} \rho_\mu \rho_\nu \langle \mu | c_i^\dagger c_j(t) | \nu \rangle \langle \nu | c_j^\dagger(t) c_i | \mu \rangle. \quad (\text{A5})$$

By contrast, the desired modulus square of the thermal Green's function would be

$$|\langle c_i(t)^\dagger c_j \rangle|^2 = \sum_{\mu\nu} \rho_\mu \rho_\nu \langle \mu | c_i^\dagger c_j(t) | \mu \rangle \langle \nu | c_j^\dagger(t) c_i | \nu \rangle. \quad (\text{A6})$$

Hence, at high temperatures, Eq. (A5) is suppressed by a factor $1/Z$, where Z is the partition sum, and thus vanishes in the thermodynamic limit. A similar reasoning applies in the case of OTO correlators.

2. Local Many-Body Interferometry

Interfering two system copies globally requires beam splitter operations with high fidelity, as in each measurement for systems of size L the same number of beam splitter operations have to be applied. To overcome this challenge, we introduce an alternative protocol that is scalable since it only requires two beam splitter operations irrespective of the system size.

A local beam splitter operation on site l is realized by coupling the left and the right copy of the quantum system by a

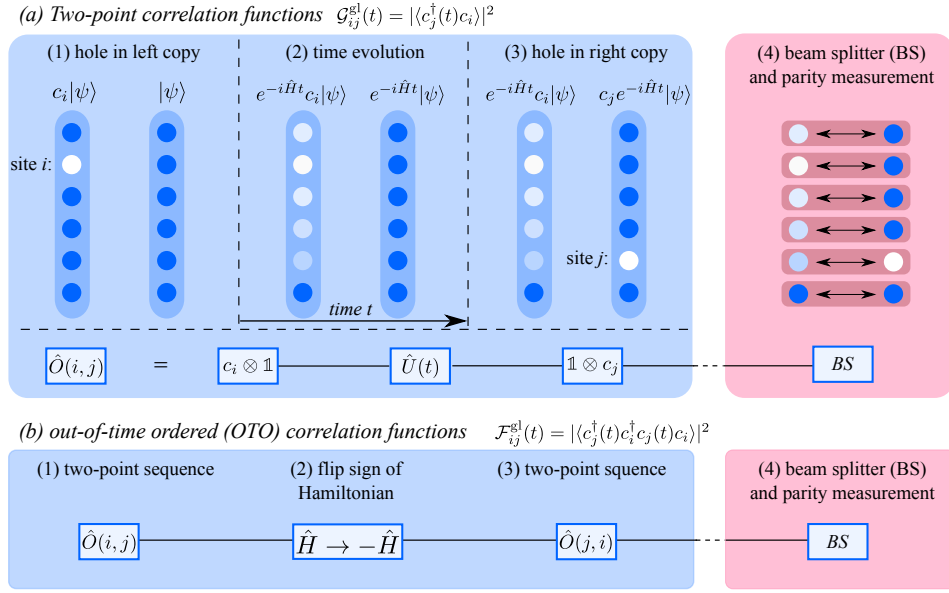


FIG. 9. **Probing dynamical correlation functions through the global interference of two many-body states.** Schematic illustration of the experimental protocol to determine the (a) time-ordered Green's function $\mathcal{G}_{ij}^{\text{gl}}(t) = |\langle c_j^\dagger(t)c_i | \psi \rangle|^2$ as well as (b) OTO correlation functions $\mathcal{F}_{ij}^{\text{gl}}(t) = |\langle \psi | c_j^\dagger(t)c_i^\dagger c_j(t)c_i | \psi \rangle|^2$. Details of the protocol are described in the text.

tunneling Hamiltonian

$$\hat{H}_l^{\text{BS}} = -J_{\text{BS}}(a_l^\dagger b_l + b_l^\dagger a_l), \quad (\text{A7})$$

where a_l^\dagger (b_l^\dagger) creates a particle in the left (right) system. The unitary evolution under Eq. (A7), $\text{BS}_l(\tau) = \exp[-i\hat{H}_l^{\text{BS}}\tau]$, for time $\tau_{\text{BS}} = \pi/4J_{\text{BS}}$ defines a 50%-50% beam splitter operation

$$\begin{pmatrix} \bar{a}_l \\ \bar{b}_l \end{pmatrix} = \underbrace{\frac{1}{\sqrt{2}} \begin{pmatrix} 1 & -i \\ -i & 1 \end{pmatrix}}_{=\text{BS}_l} \begin{pmatrix} a_l \\ b_l \end{pmatrix}. \quad (\text{A8})$$

Furthermore, the phase of the beam splitter can be adjusted by applying a field gradient between the left and the right system $\hat{H}_l^{\text{F}} = \frac{\hbar}{2}(b_l^\dagger b_l - a_l^\dagger a_l)$ for a duration τ_f , $R(\tau_f) = \exp[-i\hat{H}_l^{\text{F}}\tau_f]$:

$$\overline{\text{BS}}_l = R^\dagger(\phi) \text{BS}_l R(\phi) = \frac{1}{\sqrt{2}} \begin{pmatrix} 1 & -ie^{-i\phi} \\ -ie^{i\phi} & 1 \end{pmatrix}, \quad (\text{A9})$$

where $\phi = h\tau_f$.

The time ordered Green's function for a system prepared in an arbitrary density matrix can be measured by the following sequence (Fig. 10): (1) apply a beam splitter operation on site i for a short duration $\tau_{\text{BS}} \ll 1$. In that limit, the unitary evolution can be linearized $\text{BS}_i(\tau) = 1 - i\hat{H}_i^{\text{BS}}\tau + O(J_{\text{BS}}^2\tau^2)$. (2) Let the two copies evolve for the physical time t . (3) Apply a 50%-50% beam splitter operation on site j with a phase that is detuned from the first one by $\phi = \pi/2$. (4) Finally, the density difference $\delta\bar{n}_j$ between the right and the left subsystem is

measured. This leads to the following measurement outcome

$$\mathcal{G}_{ij}^{\text{loc}}(t) = \langle \text{BS}_i^\dagger(\tau) e^{i\hat{H}t} \overline{\text{BS}}_j^\dagger \delta\bar{n}_j \overline{\text{BS}}_j e^{-i\hat{H}t} \text{BS}_i(\tau) \rangle. \quad (\text{A10})$$

We first calculate the densities after the beam splitter operation $\overline{\text{BS}}_j$, which gives

$$\bar{n}_{l,j} = \bar{a}_j^\dagger \bar{a}_j = \frac{1}{2}(a_j^\dagger - b_j^\dagger)(a_j - b_j) \quad (\text{A11a})$$

$$\bar{n}_{r,j} = \bar{b}_j^\dagger \bar{b}_j = \frac{1}{2}(a_j^\dagger + b_j^\dagger)(a_j + b_j). \quad (\text{A11b})$$

Computing the density difference between the right and the left system, we find

$$\delta\bar{n}_j = \bar{n}_{l,j} - \bar{n}_{r,j} = -(b_j^\dagger a_j + a_j^\dagger b_j). \quad (\text{A12})$$

Considering now that the duration of the first beam splitter operation on site i is short and using the particle number conservation, we obtain

$$\mathcal{G}_{ij}^{\text{loc}}(t) = 4J_{\text{BS}}\tau \text{Im}\{\langle a_j^\dagger(t)a_i \rangle \langle a_j(t)a_i^\dagger \rangle\} + O(J_{\text{BS}}^3\tau^3). \quad (\text{A13})$$

The conventional time ordered one-body correlation function is defined as $\mathcal{G}_{ij}(t) = \langle a_j^\dagger(t)a_i \rangle$. In our protocol, the imaginary part of the product of a particle and a hole correlation function is measured. However, we argue below that this observable carries related information as the time-ordered correlation function $\mathcal{G}_{ij}(t)$; see also Fig. 11 (b).

OTO correlators are measured by a straight forward extension; Fig. 10 (b): (1) Apply a beam splitter operation for a short duration $\tau_{\text{BS}} \ll 1$ at site i . (2) Let the system evolve for a physical time t . (3) Use single-site addressing to remove a particle on site j in both copies. (4) Flip the sign of the

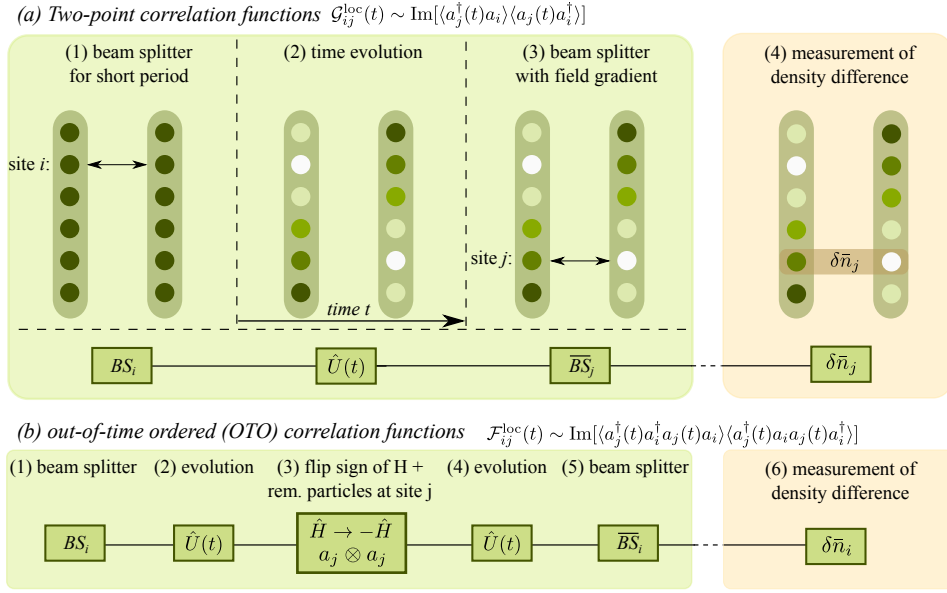


FIG. 10. **Probing dynamical correlation functions through the local interference of two many-body states.** Using local beam-splitter operations only, our protocol measures (a) time ordered correlator $\mathcal{G}_{ij}^{\text{loc}}(t) \sim \text{Im}[\langle a_j^\dagger(t) a_i \rangle \langle a_j(t) a_i^\dagger \rangle]$ as well as (b) the OTO correlator $\mathcal{F}_{ij}^{\text{loc}}(t) \sim \text{Im}[\langle a_j^\dagger(t) a_i^\dagger a_j(t) a_i \rangle \langle a_j^\dagger(t) a_i a_j(t) a_i^\dagger \rangle]$. A detailed description of the protocol is given in the text.

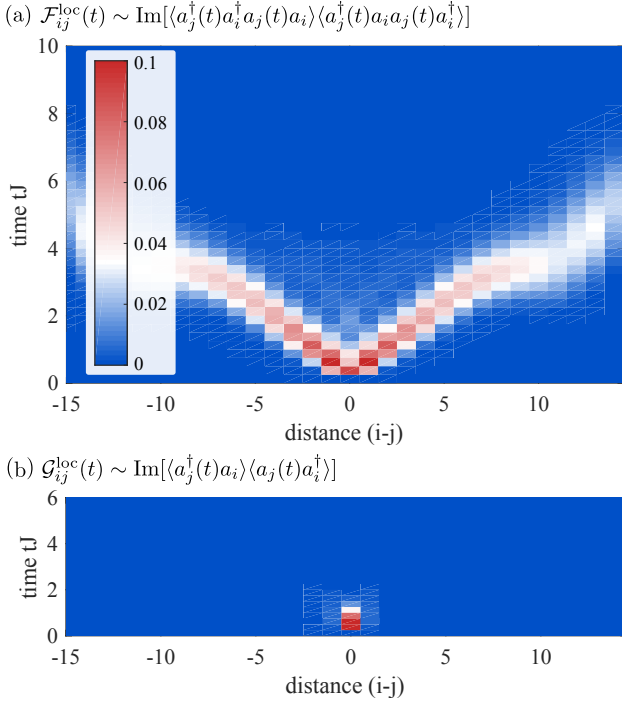


FIG. 11. **Correlation functions obtained from the local interference of two quantum states.** (a) OTO correlation functions $\mathcal{F}_{ij}^{\text{loc}}(t)$ and (b) time-ordered correlation functions $\mathcal{G}_{ij}^{\text{loc}}(t)$ as measured by the protocol based on local beam splitter operations (Sec. A 2) contain similar information as the originally introduced correlators. The data is shown for temperature $T = 4J$, interactions $U = J$, chemical potential $\mu = 0$, and systems of size $L = 30$ and can thus be compared to Fig. 1.

Hamiltonian $\hat{H} \rightarrow -\hat{H}$, as suggested in the previous section. Let the system evolve in time for the duration t . (5) Apply the 50%-50% beam splitter operation $\overline{\text{BS}}_i$ on site i . Evaluating these steps, we find

$$\begin{aligned} \mathcal{F}_{ij}^{\text{loc}}(t) &= \langle \text{BS}_i^\dagger(\tau) e^{i\hat{H}t} a_j^\dagger b_j^\dagger e^{-i\hat{H}t} \overline{\text{BS}}_i^\dagger \delta \bar{n}_i \rangle \\ &\quad \times \langle \overline{\text{BS}}_i e^{i\hat{H}t} a_j b_j e^{-i\hat{H}t} \text{BS}_i(\tau) \rangle \\ &= 4J_{\text{BS}} \tau \text{Im} \{ \langle a_j^\dagger(t) a_i^\dagger a_j(t) a_i \rangle \langle a_j^\dagger(t) a_i a_j(t) a_i^\dagger \rangle \} + O(J_{\text{BS}}^3 \tau^3). \end{aligned} \quad (\text{A14})$$

This expression corresponds to the product of two OTO correlation function. Four point correlators in spin systems can be obtained with related protocols [18].

The OTO correlator $\mathcal{F}_{ij}^{\text{loc}}(t)$ obtained from local interference contains at the considered temperatures essentially the same information as the one we originally introduced. As the protocol measures the imaginary part of a product of two OTO correlators, it starts out at zero. The scrambling across the quantum state manifests itself in the linear propagation of a wave-packet in $\mathcal{F}_{ij}^{\text{loc}}(t)$ [see Fig. 11 (a)] from which light-cone and butterfly velocities can be extracted. In Fig. 11 (a), we once again attribute the superballistic spread of information, which kicks in at $|i - j| \gtrsim 7$, to the finite MPO bond dimension of 400. Similarly, $\mathcal{G}_{ij}^{\text{loc}}(t)$ starts off at zero but then develops a peak that quickly decays; Fig. 11 (b). From that we determine the quasiparticle lifetime $\tau J \sim 0.32$ which corresponds roughly to half the lifetime obtained for the Green's function $\mathcal{G}_{ij}(t)$. This factor can be attributed to the fact that here the product of two correlation functions is measured.

With the protocols discussed so far, static one-body correlation functions can be measured by setting the physical time $t = 0$. Moreover, a generalization of the local protocol makes

it possible to measure static correlations functions of *arbitrary* order. Specifically, correlators of $\delta\bar{n}_i$ determine one-body correlation functions of the original many-body state:

$$\langle \delta\bar{n}_i \delta\bar{n}_j \rangle = 2 \langle a_i^\dagger a_j \rangle \langle a_i a_j^\dagger \rangle. \quad (\text{A15})$$

Here we used that the left and the right initial states are identical. Higher order static correlation functions in the creation a_i^\dagger and annihilation operators a_i are straightforwardly obtained by measuring higher order correlators in $\delta\bar{n}_i$. We emphasize that this protocol scales favorable with system size, and that correlators between arbitrary sites and of arbitrary order can be taken in a single shot by performing the beam splitter operations on the full system.

The density matrix describing the quantum state of a system can be expressed as

$$\hat{\rho} = \mathcal{N} \sum_{i_1, \dots, i_N} r_{i_1, \dots, i_N} \hat{\sigma}_{i_1} \otimes \dots \otimes \hat{\sigma}_{i_N}, \quad (\text{A16})$$

where \mathcal{N} is a normalization constant and the $\hat{\sigma}_{i_j}$ constitute a suitable basis [52]. In the case of fermions or hard-core bosons, one possible choice for the basis are the Pauli matrices. The knowledge of correlators up to sufficient order makes it possible to determine the so-called Stokes parameters r_{i_1, \dots, i_N} and thereby to reconstruct the density matrix, which paves the way for the full state tomography of quantum states with massive particles.

3. Measuring Dynamical Density Correlators

In this section we discuss two different possibilities to measure dynamical density correlation functions and thereby observe their diffusive behavior.

The dynamic structure factor $S(k, \omega)$, which is the spatial and temporal Fourier transform of the density correlator $C_n(x, t)$, can be measured with Bragg spectroscopy [53, 54]. In Bragg spectroscopy, the detuning of the two laser beams sets the frequency ω and the angle between the beams the transferred momentum k . A measurement of the absorption of the system as a function of k and ω directly maps out the dynamic structure factor $S(k, \omega)$. Diffusion manifests itself in the wavevector and frequency resolved structure factor $S(k, \omega)$ as Lorentzian peaks with half-width-half-maximum that scales as Dq^2 .

It is furthermore possible to measure the dissipative response $\langle [n_i(t), n_j] \rangle$ to a local perturbation of the system in a quantum gas microscope. To this end, a local potential $\delta H = n_j \delta \mu$ is created at site j by applying a laser for a short time τ , yielding the time evolution $\exp[-i\delta H \tau] \sim 1 - i\delta H \tau + O(\delta \mu^2 \tau^2)$. Measuring the density at site i after the unitary time evolution for duration t we obtain

$$\chi_{ij}^{\text{loc}}(t) = \langle n_i(t) \rangle + i\delta \mu \tau \langle [n_i(t), n_j] \rangle + O(\delta \mu^2 \tau^2). \quad (\text{A17})$$

In equilibrium, the fluctuation-dissipation theorem provides an exact relation between $\langle [n_i(t), n_j] \rangle$ and $\langle n_i(t) n_j \rangle$. The accurate measurement of the former therefore enables the observation of diffusive response in the dynamical density correlator.